Article

Research on the Influence of Subway Tunnel Depth on Heat Storage Characteristics of the Surrounding Soil Mass

Huaitao Song *[ID]**, Jingfen Li, Yueyang Yu and Qianlong Chen**

School of Building Environment Engineering, Zhengzhou University of Light Industry, Zhengzhou 450001, China; lijingfen@email.zzuli.edu.cn (J.L.); yuyueyang@email.zzuli.edu.cn (Y.Y.); chenqianlong@email.zzuli.edu.cn (Q.C.)
* Correspondence: songhuaitao@zzuli.edu.cn

Abstract: With the long-term running of the subway, the soil layer around the tunnel takes on the thermal deposition effect, which can lead the air in the tunnel to heat up and pose a serious threat to the safety operation of trains. Through taking some subway tunnels from typical zones as an example, the influence of tunnel depth on the heat storage characteristics of the surrounding soil mass was analyzed in the paper. The results indicate that the temperature field of the surrounding soil mass was thermally disturbed by both the ground air temperature and the tunnel air temperature, and there was a significant coupling point 'O' located at the center of the tunnel overburden. With the extension of the heat-exchange time, the shape of the cooling ring around the tunnel gradually changed from a circle to an oval. For the analysis of cases, from the space aspect, when the tunnel depth was less than 30 m, the wall temperature increased gradually with the increase of tunnel depth. From the time aspect, over time, the wall temperature gradually rose and finally reached a fixed value. From the region aspect, the heat absorption capacity of different areas decreased gradually with the increase of tunnel depth. When the depth exceeded 45 m, the heat absorption capacity of certain cities became negative. In addition, three typical boundaries were discussed, and the optimal method for evaluating the heat absorption capacity of the tunnel soil was ultimately determined. This study has important reference value for temperature control and positioning problems in the process of tunnel construction and operation.

Keywords: subway tunnel; soil mass; tunnel depth; thermal deposition effect; finite volume method

1. Introduction

With the rapid development of urbanization, subways are playing an increasingly important role in alleviating and improving urban traffic congestion [1]. However, the soil mass surrounding the tunnel can generate a thermal deposition effect during subway operation, which inevitably results in an annual increase in tunnel air temperature [2–4]. For example, the platform temperature of Beijing Subway Line 1 has risen from 23.5 °C to 28.5 °C over the past 40 years, and the highest temperature has reached 31 °C in summer [5,6]. On London's Central Line, it was reported that the carriage temperature exceeded 40 °C, making it unbearable for passengers [7,8]. The deteriorating thermal environment of the subway inevitably affects the comfort of the operating environment, the efficiency of the air-conditioning system, and the stability of the tunnel surrounding structure; this can seriously threaten safe and stable operation of the subway [9,10]. Therefore, it is essential to study the thermal transport law of tunnel surrounding soil mass.

According to Li [11], subways are typically constructed at depths ranging from 20 m to 50 m below ground level. However, due to geological conditions, excavation periods, economic costs, the prevention of nuclear war, or other factors, the depth of underground tunnels varies among different countries and regions. Lian [12] mentioned that many stations in the St. Petersburg subway are more than 60 m deep. The deepest station in Hong Kong's subway is the Hong Kong University Station on the Island Line, which is over 70 m

deep. Kiev Metro Line 1's Arsenal station is located in the middle of a mountain, about 105.5 m away from the ground. The Pyongyang subway in North Korea is the deepest subway system in the world, with a depth of 200 m at its lowest point.

The thermal environment of the subway is influenced by many factors, with the storage and release of heat from the tunnel soil layer being the main factors. Its formation mechanism and heat migration law have been deeply studied both in China and abroad [13–15]. In theoretical analysis, the analytical solution for the heat transfer equations of the soil mass was derived [16–21], but the complexity of the solution expression greatly limits its application in engineering. In addition, due to the rapid development of numerical calculation methods, the heat transfer rules of the soil mass surrounding the tunnel have been widely studied from various perspectives, such as mechanical ventilation systems [22–25], heat absorption ratio [26], capillary heat exchange [27], tunnel temperature assessment [28], heat storage effects [29], seasonal heat storage characteristics [30–35], and thermal physical parameters [36–41]. Therefore, the heat transfer characteristics of the tunnel soil layer have been systematically discussed above. However, there is a lack of relevant research on the underground depth that impacts the thermal perturbation effect from both ground air and tunnel air.

This paper is structured as follows: First, a numerical model is established for heat conduction of the soil mass based on the principle of energy conservation. Second, the governing equations of the heat transfer of tunnel soil mass are numerically solved by the finite volume method, and the experimental results verify the effectiveness of this model. Finally, the influence of tunnel depth on the heat storage characteristics of the surrounding soil mass is discussed in detail. This study helps us to better understand the influence of tunnel depth, ground air, and tunnel air on the thermal transport law of the soil mass surrounding the tunnel.

2. Formulation of the Problem

2.1. Physical Model

To simplify the heat transfer problem, the following assumptions were proposed: (i) The soil layer around the tunnel was homogeneous and isotropic, with no internal heat sources; (ii) the tunnel section had a circular shape; (iii) the axial heat flow transfer was neglected, simplifying the three-dimensional heat conduction of the subway tunnel to a two-dimensional plane problem; (iv) the temperature fluctuation were not taken into consideration, and the annual average temperatures of both ground and tunnel air were used as boundary conditions; (v) the thermal properties did not vary with temperature; (vi) the latent heat and thermal radiation of the tunnel surrounding rock wall were not considered.

Based on the above assumptions, this model is subject to four boundary conditions as shown in Figure 1. Γ_1 and Γ_2 represent the boundaries for convective heat transfer; Γ_3 denotes the adiabatic boundary of temperature field; and Γ_4 signifies the raw soil layer temperature. H is the depth of the metro tunnel.

In addition, the soil mass surrounding the tunnel was discretized using unstructured triangular mesh elements, resulting in a total of 3130 cells and 1630 nodes. The closer the grid element is to the tunnel wall or boundary of the calculation domain, the smaller its size in the calculation area becomes. This effectively improves both the accuracy and speed of the program.
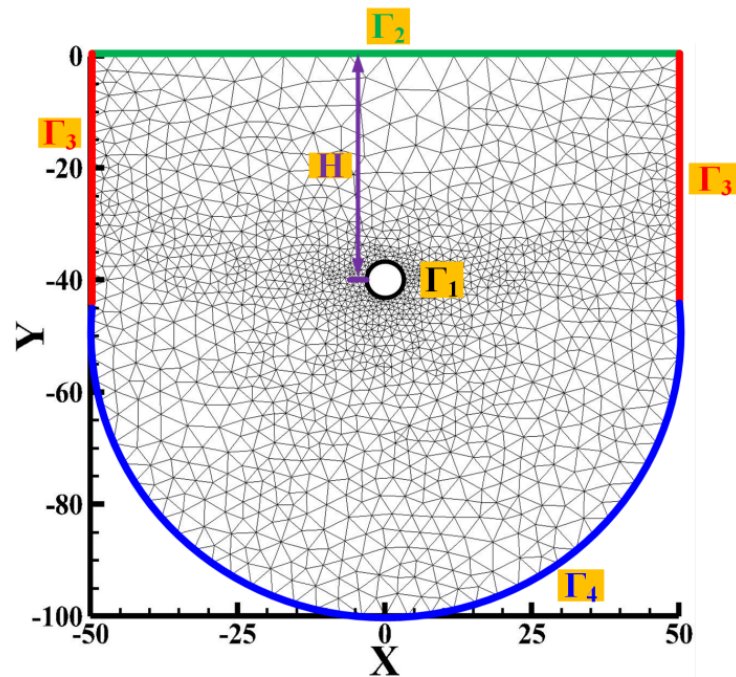
Figure 1. Unstructured grid division of the physical model.

2.2. Mathematical Model

The integral equation for heat transmission in tunnel soil mass is written as follows [37]:

$$-\iint_S \lambda(\frac{\partial^2 T}{\partial x^2} + \frac{\partial^2 T}{\partial y^2})dS = \iint_S (\rho C_P \frac{\partial T}{\partial t})dS \tag{1}$$

where T is the temperature field of the soil mass (°C); λ is the heat conductivity coefficient of the soil mass (W/(m•°C)); ρ is the density of the soil mass (kg/m^3); C_p is the specific heat capacity of the soil mass (J/(kg•°C)); x and y are the Cartesian coordinates (m); t is the transmitting time (s); and S is the area of the integration domain (m^2).

The boundary conditions:

$$\begin{cases} \lambda\frac{\partial T}{\partial n}\Big|_{\Gamma_1} = -h_M(T|_{\Gamma_1} - T_{Mf}) \\ \lambda\frac{\partial T}{\partial n}\Big|_{\Gamma_2} = -h_G(T|_{\Gamma_2} - T_{Gf}) \\ q|_{\Gamma_3} = 0 \\ T|_{\Gamma_4} = T_{gu} \end{cases} \tag{2}$$

where h_M is the convection heat-exchange factor of the tunnel wall-air (W/(m^2•°C)); h_G is the convection heat-exchange factor of the ground surface-air (W/(m^2•°C)); T_{Mf} and T_{Gf} are the air temperature in the tunnel and on the ground, respectively (°C); T_{gu} is the raw temperature of the soil mass (°C), and q is the heat flux density on the tunnel wall (W/m^2).

The initial condition:

$$T|_{t=0} = T_{gu} \tag{3}$$

The physical and mathematical models above constitute the foundation for simulating the heat conduction of the soil mass surrounding the tunnel.

3. Solution of Governing Equation

3.1. Discretization Model

Qin et al. [42,43] proposed that the heat transfer problem can be solved using the finite volume method. It can be expressed in the matrix form as follows:

$$\left\{ \begin{array}{c} \Theta_i^e \\ \Theta_j^e \\ \Theta_m^e \end{array} \right\} = \begin{bmatrix} k_{ii} & k_{ij} & k_{im} \\ k_{ji} & k_{jj} & k_{jm} \\ k_{mi} & k_{mj} & k_{mm} \end{bmatrix} \left\{ \begin{array}{c} T_i \\ T_j \\ T_m \end{array} \right\} - \begin{bmatrix} n_{ii} & n_{ij} & n_{im} \\ n_{ji} & n_{jj} & n_{jm} \\ n_{mi} & n_{mj} & n_{mm} \end{bmatrix} \left\{ \begin{array}{c} \frac{\partial T_i}{\partial t} \\ \frac{\partial T_j}{\partial t} \\ \frac{\partial T_m}{\partial t} \end{array} \right\} \tag{4}$$

where $k_{ll} = -\lambda_e(b_l^2 + c_l^2)/3\Delta$; $k_{ln} = k_{nl} = -\lambda_e(b_l b_n + c_l c_n)/3\Delta$; $n_{ll} = \frac{20\Delta}{81}\rho_e c_e$; $n_{ln} = n_{nl} = \frac{8\Delta}{81}\rho_e c_e$; $l, n = i, j, m$, and $l \neq n$; T_i, T_j, and T_m represent the node (i, j, m) temperature; Θ_i^e, Θ_j^e, and Θ_m^e represent the node (i, j, m) contribution from the e_{th} element; and e represents the local element.

Zhang et al. [44] presented that the heat conduction problem has three main types of boundaries. As shown in Figure 1, the fluid-solid heat transfer boundaries Γ_1 and Γ_2 are called the Robin boundary condition; the boundary Γ_3 is defined as the adiabatic boundary with zero heat flux density, which is referred to as the Neumann boundary condition; and the boundary Γ_4 is called the Dirichlet boundary condition, which is a constant. The boundary grid elements are described in matrix form as follows:

$$\left\{ \begin{array}{c} \Theta_i^b \\ \Theta_j^b \end{array} \right\} = \left\{ \begin{array}{c} q_{bi}l_{bi} \\ q_{bj}l_{bj} \end{array} \right\} = \begin{bmatrix} u_{ii} & u_{ij} \\ u_{ji} & u_{jj} \end{bmatrix} \begin{bmatrix} T_i \\ T_j \end{bmatrix} - \left\{ \begin{array}{c} v_i \\ v_j \end{array} \right\} \tag{5}$$

Neumann boundary condition:

$$u_{ii} = u_{ij} = u_{ji} = u_{jj} = 0; \ v_i = v_j = -\frac{2}{3}s_b\left(\frac{2}{3}q_i + \frac{1}{3}q_j\right)$$

Robin boundary condition:

$$u_{ii} = u_{jj} = \frac{4hs_b}{9}; \ u_{ij} = u_{ji} = \frac{2hs_b}{9}; \ v_i = v_j = \frac{2hs_bT_f}{3}$$

where q_i and q_j represent the heat flux density at nodes i and j (W/m^2); s_b is the length between node i and node j; h is the convection coefficient (W/(m^2•°C)); and T_f is the air temperature (°C).

3.2. Program Design

A computer program was compiled using Visual Basic language to simulate transient heat conduction of the tunnel soil mass. The program was able to solve a system of linear equations at each time point using the Gauss-Seidel iterative method, and the time step calculated by equal proportion was 1.1. The Origin and Tecplot 360 EX 2017 software were employed to post-process the numerical results. The flow chart of the program is shown in Figure 2.

3.3. Model Validation

The project team constructed a small experimental platform to conduct a 4 h indoor temperature field test. As shown in Figure 3, the experimental model platform consisted of three systems: the air temperature control system, the simulation experimental system, and the temperature monitoring system. The soil was poured into a sealed box with dimensions of 600 mm × 600 mm × 400 mm to simulate the soil layer surrounding the tunnel. The surrounding soil mass had a thermal conductivity of 0.244 W/(m•°C), a specific heat capacity of 975.3 J/(kg•°C), and a density of 1124.2 kg/m^3. The walls of the box were made of 2 mm-thick steel and wrapped with 10 mm thick insulation. A copper tube with a diameter of 60 mm was placed in the center of the box to circulate air. The rate of convection

heat transfer rate was 31.5 W/(m²•°C). The initial temperature field was 32.5 °C, and the recycled air temperature was maintained at 50 °C. Figure 4 shows that the model profile of the soil layer around the subway tunnel, and the typical 4 monitoring points were uniformly arranged in the model space. Point 1 from the wall was 10 mm, and the radial interval between points was 40 mm. The established heat conduction model was used for numerical analysis, and Figure 5 shows that the numerical results at different times are essentially consistent with the experimental results.
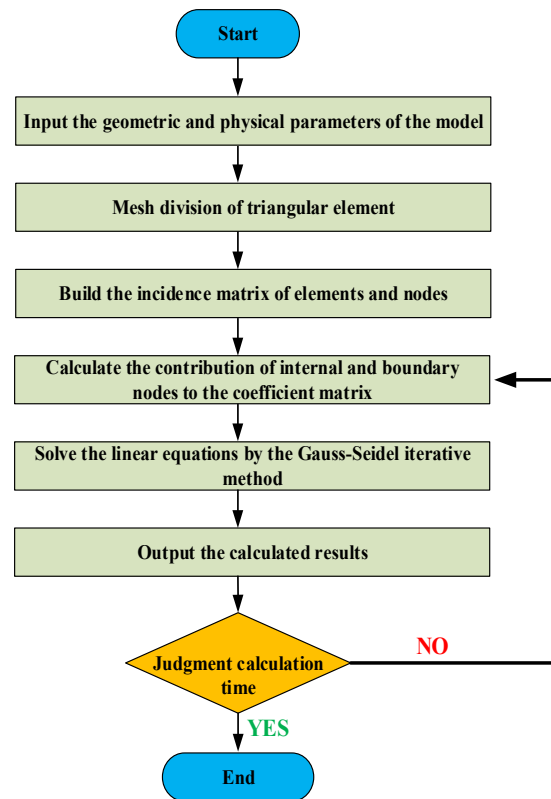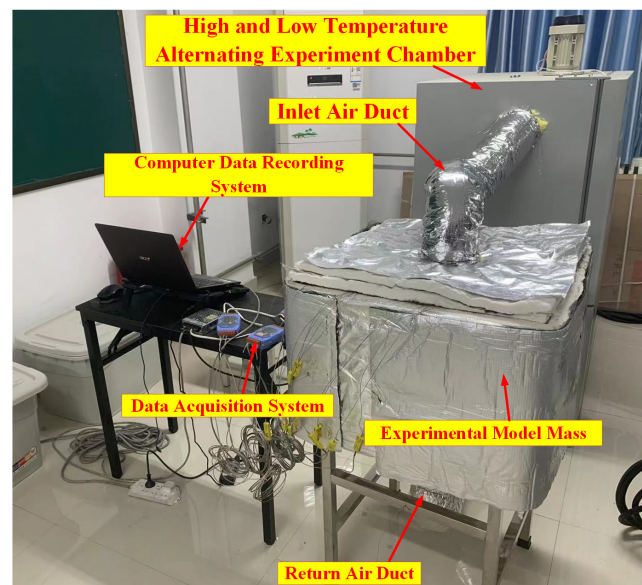

Figure 2. Program flow chart.

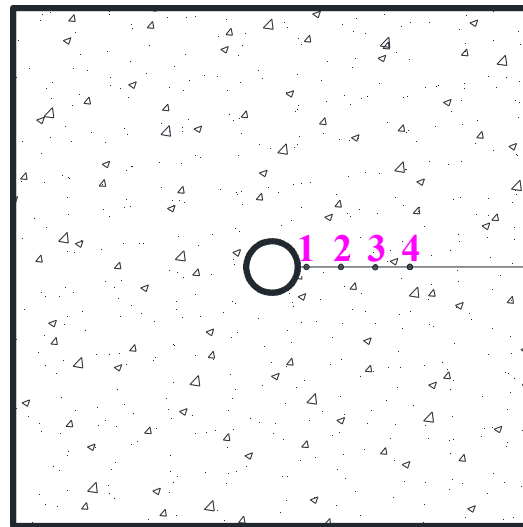**Figure 3.** Experimental system sketch.

Figure 4. Cross-section of the tunnel soil layer and temperature measurement points.
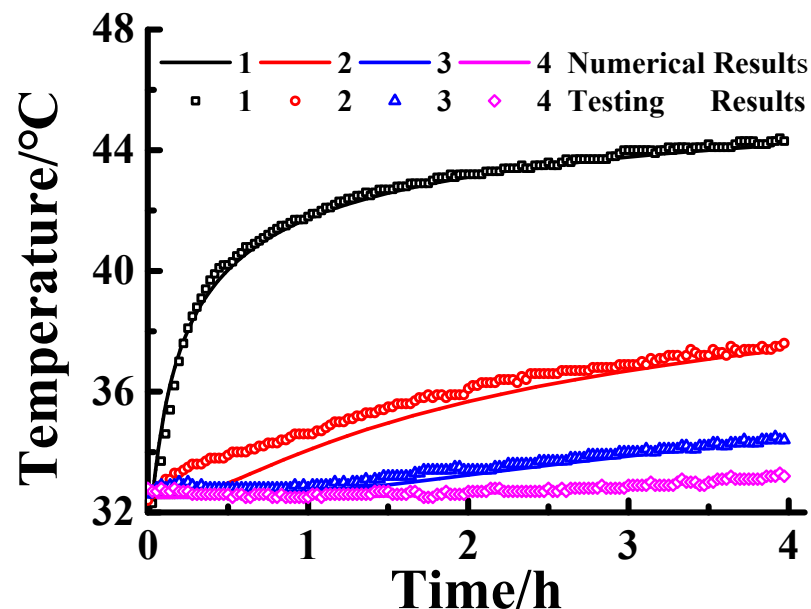

Figure 5. Comparison analysis between the numerical calculations and testing results.

3.4. Model Parameters

China is classified into five climatic zones: the Severe Cold Zone, Cold Zone, Hot-Summer Cold-Winter Zone, Hot-Summer Warm-Winter Zone, and Temperate Zone [45]. In this study, five typical cities were selected to calculate the thermal deposition effect of surrounding soil mass based on climate zoning and geographical distribution, namely Harbin, Beijing, Xi'an, Shanghai, and Shenzhen. In Figure 1, the tunnel has a radius of 3 m, the wind speed in the tunnel is 6 m/s, and the air temperature in the tunnel is 25 °C [46]. Table 1 presents the correlation parameters between tunnel soil and ground air in the aforementioned cities. Yang et al. [47] presented that the ground air speed refers to the local meteorological data in its area, and the initial temperature of tunnel soil mass is defined as 3 °C higher than the annual mean temperature of ground air. In addition, both the Dittus-Boelter equation and empirical formula were used to calculate the heat transfer convection coefficient [48,49].

Table 1. Model parameters [41].

Area	Soil Property	Density	Specific Heat Capacity	Heat Conductivity Coefficient	Mean Temperature of Ground Air	Initial Temperature of Tunnel Soil	Ground Wind Speed
		kg/m3	J/(kg•°C)	W/(m•°C)	°C	°C	m/s
Harbin	Silty Clay Loam	1850	1750	1.20	6.6	9.6	4.1
Beijing	Sandy Loam	2300	1350	1.70	14.0	17.0	3.0
Xi'an	Silt Sand	1820	1600	1.30	15.6	18.6	1.8
Shanghai	Silty Clay	1788	1940	1.02	18.5	21.5	3.8
Shenzhen	Sandy Clay Loam	2650	1050	2.10	23.2	26.2	3.1

4. Results

4.1. Temperature Distribution in Soil Mass Surrounding the Tunnel

The heat exchange among the ground air, tunnel air, and surrounding soil mass belongs to the unsteady convection heat transfer. Taking the Beijing subway tunnel for analysis, Figure 6 shows that the temperature distribution of the soil mass surrounding the tunnel at the depth of 40 m changes at four typical time points. It can be observed that the original temperature distribution of the soil mass is disturbed vertically by ground air temperature and circumferentially by tunnel air temperature, respectively. When the heat-exchange time is less than 5 years, the influence of ground air and tunnel air continues to extend deeper. When the heat-exchange time exceeds 5 years, these disturbances exhibit a remarkable coupled superposition effect in the tunnel overburden. For example, as can be seen from Figure 6d, this superimposed effect is particularly significant at the depth of 20 m. However, this effect is not evident in the underlying strata, meaning that the ground air has a limited impact on the temperature field of underground soil mass.
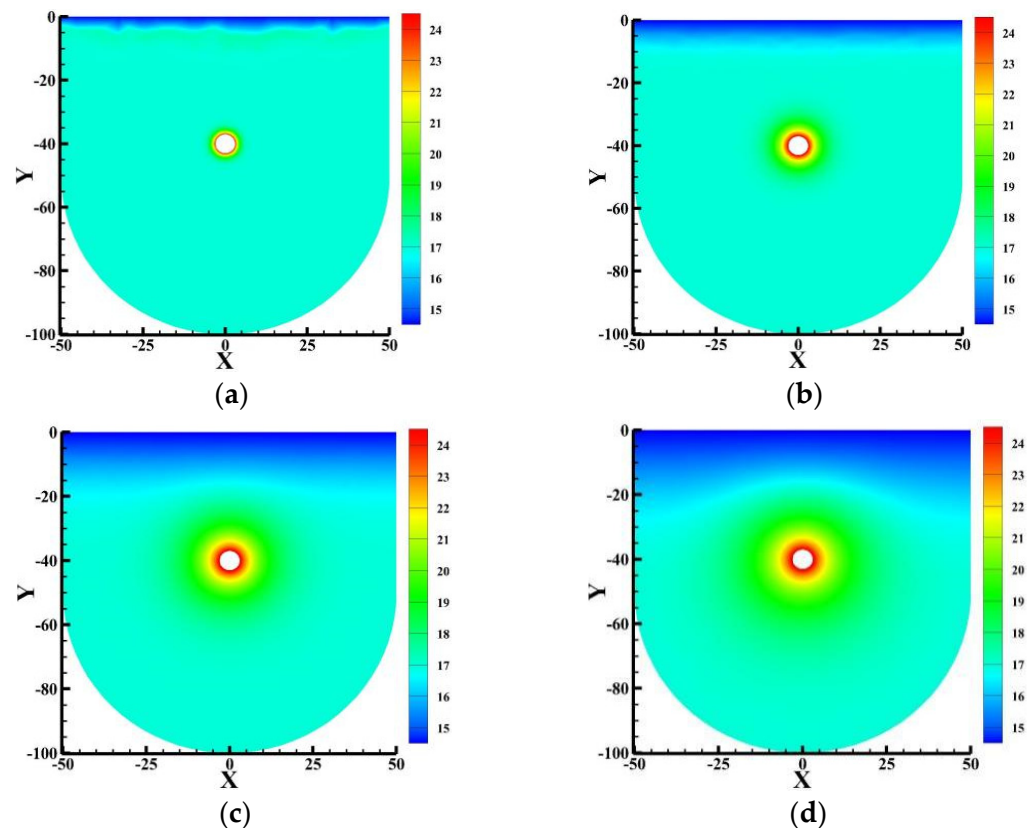
Figure 6. Temperature fields of the tunnel soil layer at different time points (unit: °C). (**a**) 1 month; (**b**) 1 year; (**c**) 5 years; (**d**) 10 years.

4.2. Temperature Distribution along the Axis of Symmetry

Figure 7 shows the temperature variation curves along the vertical symmetry axis in cross-sections of the subway tunnel at depths of 20 m, 40 m, and 60 m, respectively. It can be observed that during the initial stage, the temperature curve of the overlying strata of the tunnel presents a "Z-shaped" trend with increasing soil layer depth in the vertical space. It displays an inverted "L-shaped" curve in the underlying strata. Furthermore, the coupling superposition effect appears first at a tunnel depth of 20 m, followed by 40 m, and finally 60 m. The temperature of the soil layer around the tunnel is greatly influenced by both the ground air temperature and the depth at which the subway is buried. Meanwhile, the shallower the depth of the underground tunnel is, the higher the temperature of the overlying strata at that same depth is.
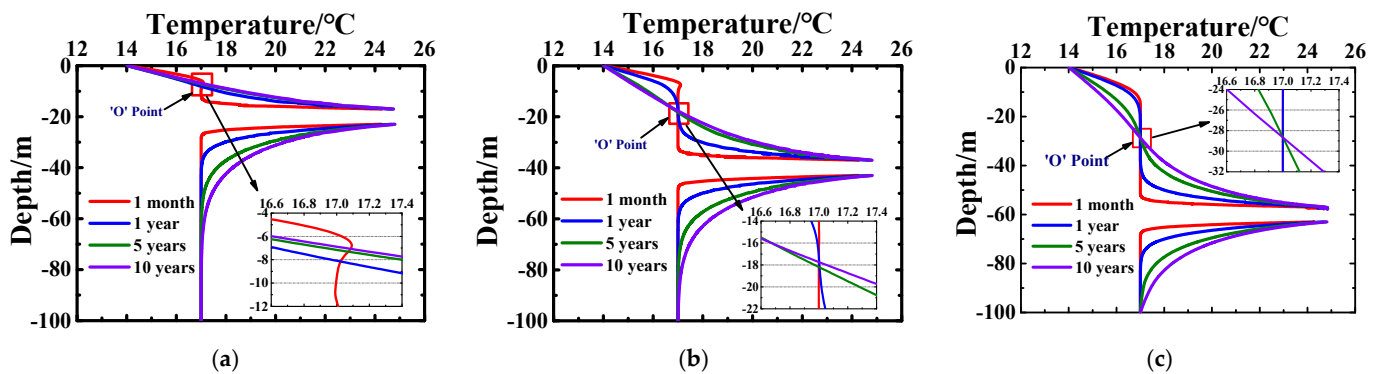

Figure 7. Temperature distribution curves of the subway tunnel cross-section. (**a**) Depth: 20 m; (**b**) Depth: 40 m; (**c**) Depth: 60 m.

Moreover, as the heat-exchange time increases, a significant coupling point 'O' emerges near the center of the overlying strata. This coupling point 'O' can be more clearly observed in the local diagram, which is located above the center. The heat transfer rate is the key factor that contributes to the position of the coupling point 'O'. According to Equation (6) [50], it is negatively proportional to both the temperature gradient and the thermal diffusivity of the body. Table 2 shows the rate of heat transfer at the coupling point 'O.' It can be seen that the rate gradually increases with time when t < 10 years. Accordingly, the shallower the depth of tunnel, the faster its heat migration velocity will be. This is because the temperature difference between the tunnel air and the original soil layer is greater than that between the ground air and the original soil layer, resulting in a higher heat transfer rate below the central point compared to above it.

$$\mathbf{v} = -\frac{\lambda}{\rho C_p}\frac{\nabla T}{T} \tag{6}$$

where v is the heat transfer rate (m/s), and ∇T is the temperature gradient (°C/m).

Table 2. The heat migration rate at the coupling point 'O'.

Cooling Time	$\triangle T$/(°C/m)	Depth: 20 m T/(°C)	V/(m/s)	$\triangle T$/(°C/m)	Depth: 40 m T/(°C)	V/(m/s)	$\triangle T$/(°C/m)	Depth: 60 m T/(°C)	V/(m/s)
the 1st month	0.027	17.020	-8.762×10^{-10}	0.001	17.000	-4.746×10^{-11}	0.000	17.000	-1.281×10^{-13}
the 1st year	−0.382	17.025	1.227×10^{-8}	−0.004	16.999	1.423×10^{-10}	0.000	17.000	5.833×10^{-13}
the 5th year	−0.556	17.483	1.740×10^{-8}	−0.149	16.826	4.853×10^{-9}	−0.036	17.022	1.142×10^{-9}
the 10th year	−0.564	17.701	1.745×10^{-8}	−0.193	16.866	6.256×10^{-9}	−0.087	17.050	2.806×10^{-9}

4.3. Ventilation Time and Cooling Rings

If the excess temperature $(T - T_{gu})$ at a point within the domain exceeds 1% of the original soil layer temperature (T_{gu}), then that point is considered to be inside the cooling ring. The mathematical expression can be written as follows:

$$\frac{T - T_{gu}}{T_{gu}} > 1\% \tag{7}$$

where $T - T_{gu}$ is the soil excess temperature (°C).

Figure 8 illustrates the temperature variation law of the cooling ring surrounding the tunnel at depths of 20 m, 40 m, and 60 m. The parameter values of those cooling-ring curves were fitted using Equation (8) and are presented in Table 3. Initially, when t < 1 year, the cooling ring takes on a circular shape, and the values of parameters A and B are almost equal. However, when t > 1 year, it gradually transforms into an oval shape, and the values of *A*, *B*, and their difference all increase over time. Meanwhile, Table 3 indicates that *A* is consistently greater than *B*. That is, the thermal disturbance velocity inside the soil body is greater in the horizontal direction than in the vertical direction. Furthermore, in terms of space, the values of parameter *A* and parameter *B* in deep tunnels are generally larger than those in shallow ones at the same time. This indicates that there is a strong correlation between the range of thermal disturbance and tunnel depth, with greater depths resulting in larger disturbance ranges.

$$\left(\frac{X - X_c}{A}\right)^2 + \left(\frac{Y - Y_c}{B}\right)^2 = 1 \tag{8}$$

where *A* is half of the length of the major axis, *B* is half of the length of the minor axis, and (*Xc*, *Yc*) denotes the center point of an elliptic equation.
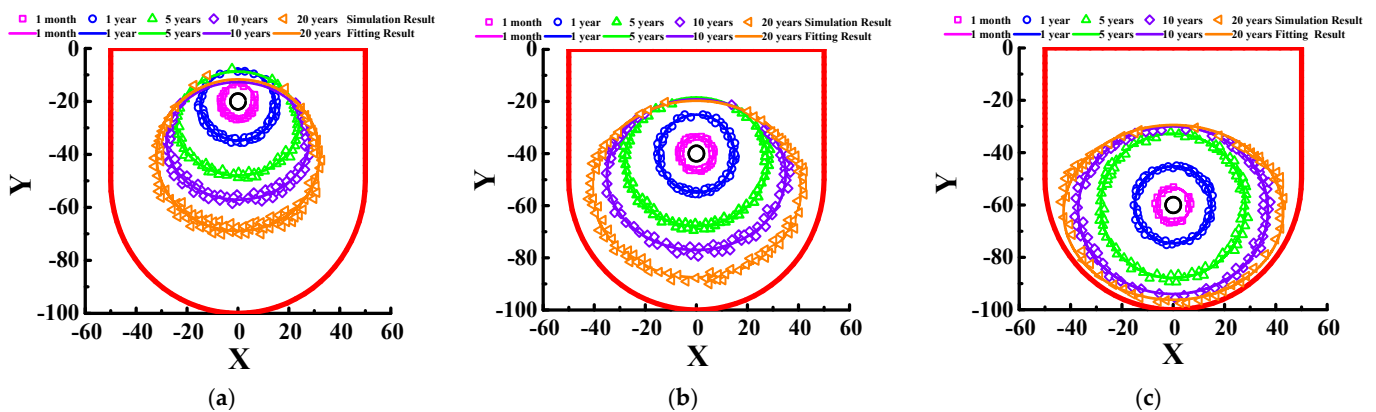

Figure 8. Ventilation time and cooling rings. (**a**) Depth: 20 m; (**b**) Depth: 40 m; (**c**) Depth: 60 m.

Table 3. The fitting parameters of the cooling ring curves around the tunnel at different times.

Cooling Time	Depth: 20 m					Depth: 40 m					Depth: 60 m				
	Xc	Yc	A	B	R^2	Xc	Yc	A	B	R^2	Xc	Yc	A	B	R^2
the 1st month	0.02	20.05	6.61	6.61	1.00	0.03	40.02	6.59	6.57	1.00	0.02	60.01	6.56	6.67	1.00
the 1st year	0.02	21.38	14.69	13.35	1.00	0.03	39.98	14.75	14.92	1.00	0.04	59.91	14.94	14.72	1.00
the 5th year	0.09	28.36	24.02	19.65	1.00	0.07	43.11	28.01	24.66	1.00	0.10	60.30	28.22	27.64	1.00
the 10th year	0.05	34.89	28.03	22.21	1.00	0.05	48.08	35.00	28.92	1.00	0.09	61.99	37.02	32.02	1.00
The 20th year	0.02	40.29	32.07	28.63	1.00	0.01	53.59	40.99	33.91	1.00	0.05	62.82	42.82	33.42	1.00

4.4. Influence of Buried Depth on the Thermal Deposition Effect of Tunnel Soil Layer

There is a distinct temperature difference between the top and bottom nodes along the tunnel wall due to the influence of the ground air, particularly in shallowly buried subways.

The inside boundary Γ_1 of the tunnel is divided into n equal units. The temperatures of the boundary nodes can be defined as $T_1, T_2, T_3, \ldots, T_n$. The length of each grid is $U_1, U_2, U_3, \ldots, U_n$, and the total perimeter is U. Thus, the circumferential temperature can be defined using a weighted average value, as expressed in the following equation.

$$\overline{T}_m = \frac{(T_1 + T_2)}{2}\frac{U_1}{U} + \frac{(T_2 + T_3)}{2}\frac{U_2}{U} + \ldots + \frac{T_n + T_1}{2}\frac{U_n}{U} \tag{9}$$

where $\overline{T}_m$ is the weighted mean temperature of internal boundary Γ_1 (°C), and U is the tunnel section perimeter (m).

Meanwhile, the amount of heat dissipation on the tunnel wall can be calculated using the Newtonian cooling formula [51]:

$$Q = h_M U(T_{Mf} - \overline{T}_m) \tag{10}$$

where Q is the heat absorption capacity per unit length (W/m).

Figure 9 shows how burial depth affects the wall temperature and heat-exchange capacity per unit length. It can be clearly observed that when H < 30 m, the wall temperature gradually increases with increasing tunnel depth, while its heat transfer capacity exhibits an opposite characteristic. However, when the tunnel depth exceeds 30 m, they are almost unaffected. Furthermore, as the ventilation time increases, the wall temperature gradually rises while its heat transfer capacity decreases. Eventually, both variables reach a fixed value after a period of heat exchange.
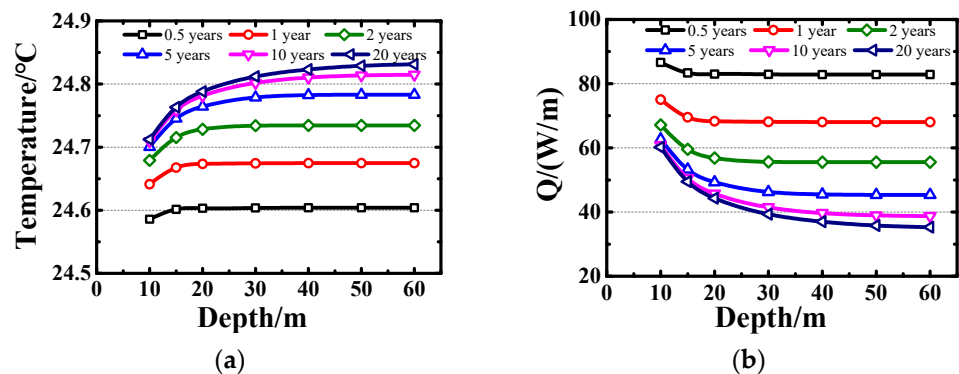
Figure 9. Variation of the tunnel wall temperature and wall heat-exchange capacity with the tunnel depth. (**a**) Tunnel wall temperature; (**b**) Tunnel wall heat-exchange capacity.

In addition, the temperature field of the soil body gradually stabilizes after the tunnel has been dug for five years. Generally, from first one to five years, the temperature on the tunnel wall is lower than that of airflow in the tunnel, which has a strong ability to absorb heat from the tunnel air. However, as the subway operation time is extended, this ability gradually decreases until it stabilizes. Therefore, it is necessary to scientifically evaluate the heat-exchange capacity between tunnel soil and air.

4.5. Evaluation of the Heat Absorption Capacity of Tunnel Soil in Typical Areas

Figure 10 displays the graphs of heat absorption capacity of the soil body under different tunnel depths for typical areas in the 50th year. It can be observed that the heat absorption capacity increases as the ground air temperature decreases, provided that the tunnel depth remains constant. However, it gradually decreases as the depth of the tunnel increases. Once the tunnel depth exceeds 45 m, such as the Shenzhen subway, its heat absorption capacity become negative. Or, for the Beijing subway, when H is 15 m, the heat absorption capacity per unit length is approximately 48.51 W/m. However, compared to H = 50 m, the absorption capacity decreases by 15.8 W/m. According to Equation (10), the power consumption of the subway can be calculated, yielding Equation (11). Therefore, if

the subway were 50 km long and operated for 30 years, its total power consumption could reach up to 2.08×10^8 KW•h.

$$\eta = QLt/\tau \tag{11}$$

where η is the power consumption (KW•h), L is the length of the tunnel in the direction of airflow (m), and t is the time (s). τ is 3,600,000, used for unit conversion.
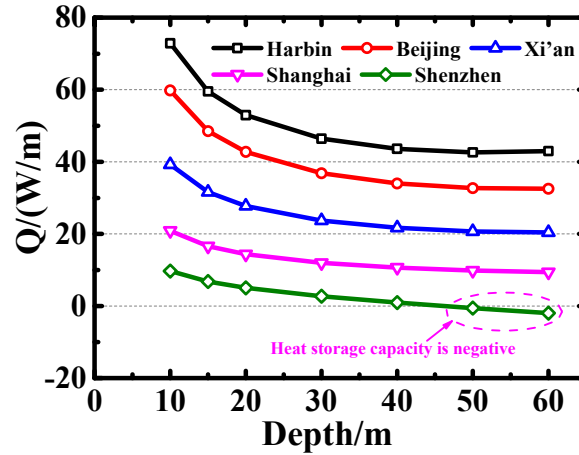

Figure 10. Curves of heat absorption capacity for tunnel walls in typical areas.

4.6. Comparison Analysis of Three Typical Models

To accurately analyze the thermal deposition effect of a tunnel soil body, constructing a precise physical model is necessary. Figure 11 depicts the schematic diagram of the physical model under three typical boundary conditions, and Table 4 summarizes the relevant contents.
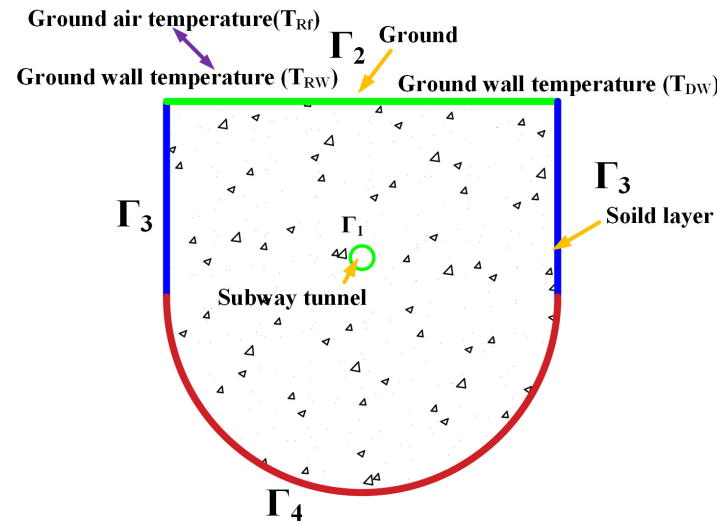

Figure 11. Typical boundary diagram.

Table 4. The settings of three typical boundary conditions.

Boundary Conditions	Case One [15,25,33–36,41]	Case Two [30,32]	Case Three [28,37]
Boundary Γ_1	Robin Boundary	Robin Boundary	Robin Boundary
Boundary Γ_2	Dirichlet Boundary	Robin Boundary	Robin Boundary
Boundary Γ_3	Dirichlet Boundary	Dirichlet Boundary	Neumann Boundary
Boundary Γ_4	Dirichlet Boundary	Dirichlet Boundary	Dirichlet Boundary

Figure 12 displays the comparison results of these three typical cases at different depths. It can be observed that the results of the calculations for case one and case two are almost identical. This indicates that as the depth of the tunnel increased, both cases yielded similar results. The main difference between these two methods is the distinct setting of the boundary Γ_2. When the ground air temperature (T_{Rf}) of the Robin boundary in case two is equal to the ground wall temperature (T_{DW}) of the Dirichlet boundary in case one, due to thermal resistance, the ground wall temperature (T_{RW}) in case two should be higher than the ground wall temperature (T_{DW}) of case one after numerical calculation. Therefore, for the shallow tunnel, the heat absorption capacity of tunnel soil layer calculated in case two is slightly smaller than that calculated in case one. However, as the tunnel depth increases, the influence of ground air temperature gradually diminishes until the results obtained by both methods converge.
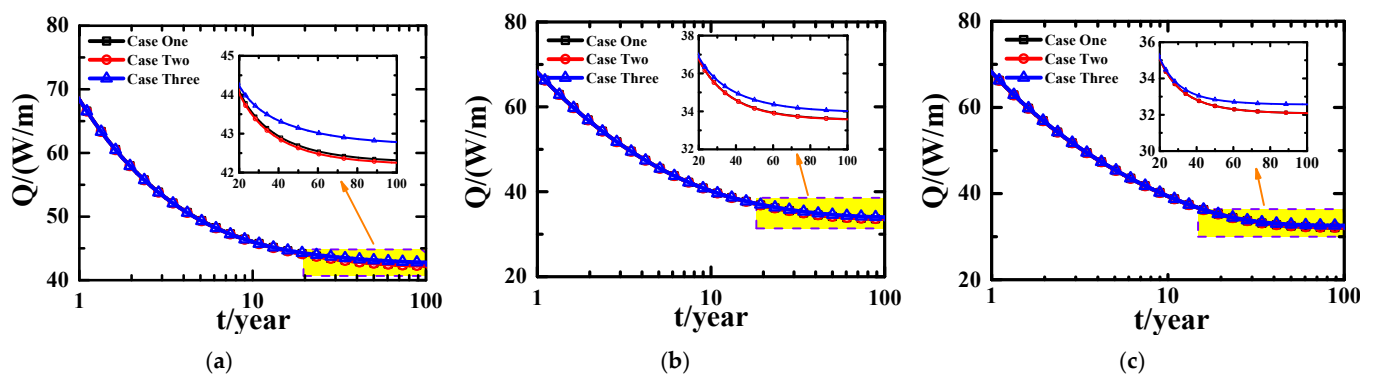
Figure 12. Curves comparing three typical cases at different depths. (**a**) Depth: 20 m; (**b**) Depth: 40 m; (**c**) Depth: 60 m.

When the time of heat exchange between the soil surrounding the tunnel and the air inside it exceeds a certain value, the amount of heat transfer calculated by case one and case two is smaller than that calculated by the third method. The reason is that the vertical boundary (Γ_3) in the third case is an adiabatic boundary, meaning there is no heat flow in or out in the horizontal direction. And in the vertical direction, the soil body only is affected by the ground air temperature. For the first two cases, the vertical boundary (Γ_3) was set as the Dirichlet boundary. However, due to the lack of consideration for the ground air temperature, there is continuous heat flowing into the computational domain in the horizontal direction, resulting in a lower long-term heat storage capacity. In general, the third kind of method should be the most consistent with reality and should be the first choice for calculation.

5. Discussions

Safety, economy, and energy efficiency are vital factors in the design and operation of subway tunnels. The paper reveals the influence of tunnel depth on the heat transfer characteristics of the surrounding soil mass. The heat storage characteristics of subway tunnel soil mass are generally consistent with the existing literatures [30,36,37]. It demonstrates a strong heat storage capacity in the initial stage, which gradually decreases over time until it reaches a stable state. In addition, on the one hand, the shallower the depth of subway tunnels, the greater the impact of ground air on the heat storage capacity of the surrounding soil mass. This is mainly reflected in two aspects: first, the thermal stress generated by the periodic ground air temperature will affect the geological safety around the tunnel; second, it poses higher requirements for the design of the subway environmental control system. On the other hand, the deeper the subway tunnel is buried, the higher the economic cost of tunnel excavation and the additional geological risk in the process of operation are. Therefore, the influence of buried depth on subway tunnel operation should be analyzed comprehensively, considering both short-term and long-term benefits.

6. Conclusions

In this work, the finite volume method was used to discuss the influence of underground depth on heat transfer law of the soil mass around the tunnel. The main conclusions are as follows:

(1) After the excavation of the tunnel, both ground air temperature and tunnel air temperature thermally disturbed the temperature field of the soil mass. Meanwhile, in the overlying soil layer of the tunnel, there was a significant coupling effect between the disturbance domain of tunnel air to the soil layer and of ground air to the soil layer. Furthermore, there was a significant coupling point 'O' located in the disturbance domain, which was situated near the center of the overlying rock layer of the tunnel. The location and time of the coupling point 'O' were greatly influenced by both the heat transfer rate of the tunnel soil body and its depth.

(2) Initially, when t < 1 year, the cooling ring around the tunnel was approximately circular in shape. Subsequently, after one year, the shape gradually transformed into an oval, and the values of the oval's parameters A and B gradually increased over time, as did the difference between them. At the same time, the range of thermal disturbance in the tunnel soil body was greater along the horizontal direction than along the vertical direction. Moreover, the parameter values of deep tunnels, A and B, were generally larger than those of shallow tunnels.

(3) In terms of space, as the depth of the tunnel increased when H < 30 m, the temperature on the tunnel wall gradually rose while its heat absorption capacity exhibited an opposite trend. However, when H > 30 m, the depth of the tunnel had almost no effect on them. In terms of time, the temperature of tunnel wall was generally lower than that of the tunnel airflow from the first one to five years, and it had a strong ability to absorb the heat emitted from the tunnel air. However, as the ventilation time increased, the temperature and heat transfer rate of the tunnel wall eventually reached a constant value.

(4) The thermal deposition effect of the soil body surrounding the tunnel was analyzed in five typical areas. The results revealed that the heat absorption capacity gradually decreased with the increase in tunnel depth across different areas. When the tunnel depth was the same, the long-term heat absorption capacity increased as the ground air temperature decreased.

(5) The study compared the heat-exchange capacity of three typical models. We found that the results of the calculations for case one and case two were almost identical, with this characteristic becoming more pronounced as the tunnel depth increased. Moreover, the heat absorption per unit length of the tunnel surrounding soil body calculated in case one and case two was lower than that calculated using the third method. According to the theory, the third method could be considered as the most accurate way to evaluate the heat absorption capacity of tunnel soil mass.

Institutional Review Board Statement: Not applicable.

Informed Consent Statement: Not applicable.

Data Availability Statement: The data used to support the findings of this study are available from the corresponding author upon request.

Conflicts of Interest: The authors declare no conflict of interest.

References

1. Hesami, S.; Ahmadi, S.; Taghavi Ghalesari, A.; Hasanzadeh, A. Ground Surface Settlement Prediction in Urban Areas due to Tunnel Excavation by the NATM. *Electron. J. Geotech. Eng.* **2013**, *18*, 1961.
2. Wang, C.; Li, C.; Xie, L.; Wang, X.; Chang, L.; Wang, X.; Li, H.X.; Liu, Y. Thermal environment and thermal comfort in metro systems: A case study in severe cold region of China. *Build. Environ.* **2023**, *227*, 109758. [CrossRef]
3. Winterling, R.; Nicholson, D.; Winter, A.; Chen, Q.; Silva, M. The design of thermal tunnel energy segments for Crossrail, UK. In Proceedings of the Institution of Civil Engineers-Engineering Sustainability; Thomas Telford Ltd.: London, UK, 2014; Volume 167, pp. 118–134. [CrossRef]
4. Ampofo, F.; Maidment, G.; Missenden, J. Underground railway environment in the UK Part 2: Investigation of heat load. *Appl. Therm. Eng.* **2004**, *24*, 633–645. [CrossRef]
5. Pan, S.; Liu, Y.; Xie, L.; Wang, X.; Yuan, Y.; Jia, X. A thermal comfort field study on subway passengers during air-conditioning season in Beijing. *Sustain. Cities Soc.* **2020**, *61*, 102218. [CrossRef]
6. Pan, S.; Wang, H.; Pei, F.; Yang, L.; Zhang, X. An Investigation on Energy Consumption of Air Conditioning System in Beijing Subway Stations. *Enrgy Proc.* **2017**, *142*, 2568–2573. [CrossRef]
7. Hu, S.; Mao, Z.; Ji, Y.; Liu, G.; Tong, Z.; Guan, Y. Numerical research on temperature field in surrounding rock during long-term operation of subway source heat pump project. *Acta Energlat Solaris Sin.* **2021**, *11*, 429–436. [CrossRef]
8. Tong, L.; Lu, S.; Ji, Y.; Hu, S.; Liu, H.; Liu, N. Research progress and key issues of waste heat utilization in subway. *J. QingDao Univ. Technol.* **2019**, *40*, 97–102. [CrossRef]
9. Wang, S.; Wang, R.; Zhu, Y. Measurement and analysis of temperature in underground space of Beijing subway. *Undergr. Space* **2002**, *22*, 339–342. [CrossRef]
10. Yu, Y.; You, S.; Zhang, H.; Ye, T.; Wang, Y.; Wei, S. A review on available energy saving strategies for heating, ventilation and air conditioning in underground metro stations. *Renew. Sust. Energ. Rev.* **2021**, *141*, 110788. [CrossRef]
11. Li, Q. The Reasonable Buried Depth of Beijing Subway Tunnels by Shallow Tunneling Method. Master's Thesis, Beijing Jiaotong University, Beijing, China, 2011.
12. Lian, Z. Study on Construction Mechanical Characteristics and Deformation Control Technology of Urban Deep Super-Long-Span Underground Space. Master's Thesis, Southwest Jiaotong University, Chengdu, China, 2021.
13. Zeng, Z.; Kuang, Y.; Gong, J.; Li, L. The analyzing of the temperature distribution in the metro tunnel. In *2014 Annual Conference on Railway Heating and Ventilation*; China Railw Society: Chengdu, China, 2014; pp. 147–156.
14. Li, Y. Study on Features of Half Covered Ground Freezing Temperature Field in Metro Tunnel. *Mine Construct Technol.* **2020**, *41*, 53–57.
15. Wang, L.; Zou, X.; Tao, H.; Liu, C.; Du, Z.; Song, J.; Zheng, Y. Experimental study on evolution characteristics of heat reservoir of wall rock in underground railway tunnels. *Hv&Ac* **2017**, *47*, 53–57.
16. Krarti, M.; Kreider, J.F. Analytical model for heat transfer in an underground air tunnel. *Energ. Convers. Manag.* **1996**, *37*, 1561–1574. [CrossRef]
17. Singh, S.; Jain, P.K.; Rizwan-uddin. Analytical solution to transient heat conduction in polar coordinates with multiple layers in radial direction. *Int. J. Therm. Sci.* **2008**, *47*, 261–273. [CrossRef]
18. Sun, T.; Luo, Z.; Chay, T. An analytical model to predict the temperature in subway-tunnels by coupling thermal mass and ventilation. *J. Build. Eng.* **2021**, *44*, 102564. [CrossRef]
19. Yang, D.; Zhang, J. Theoretical assessment of the combined effects of building thermal mass and earth–air-tube ventilation on the indoor thermal environment. *Energ. Build.* **2014**, *81*, 182–199. [CrossRef]
20. Zhou, Y.; Zhang, X.; Deng, J. A mathematical optimization model of insulation layer's parameters in seasonally frozen tunnel engineering. *Cold Reg. Sci. Technol.* **2014**, *101*, 73–80. [CrossRef]
21. Zhao, P.; Li, X.; Zhang, D.; Xu, W.; Liu, J.; Wu, W.; Deng, L. A simplified method to determine the comprehensive heat transfer quantity in subway tunnels. *Energ. Build.* **2021**, *247*, 111090. [CrossRef]
22. Zhang, Y.; Li, X. Numerical analysis on the condenser inlet air temperature of train-mounted air conditioner when a train stops in subway station tunnel. *Sustain. Cities Soc.* **2021**, *69*, 102793. [CrossRef]
23. Jiang, H.; Niu, F.; Ma, Q.; Su, W.; Wang, E.; He, J. Numerical analysis of heat transfer between air inside and outside the tunnel caused by piston action. *Int. J. Therm. Sci.* **2021**, *170*, 107164. [CrossRef]
24. Wang, L.; Du, Z.; Sun, Y.; Song, J.; Zheng, Y.; Zhang, J. Temperature Theory Model and Characteristics Analysis on Non-isothermal Coupling between Subway Platform Piston Wind and Air Jet. *Int. J. Refrig.* **2016**, *37*, 43–48. [CrossRef]
25. Yu, L.; Wu, X.; Yu, H. Effect of High frequency Thermal Disturbance on Soil Temperature around the Metro Tunnels. *J. Civ. Arch Env. Eng.* **2011**, *33*, 95–101.
26. Zhao, P.; Li, X.; Liu, J.; Zhang, D.; Qiao, H. Monitoring and analysis of the subway tunnel wall temperature and surrounding rock/soil heat absorption ratio. *Build. Environ.* **2021**, *194*, 107657. [CrossRef]
27. Ren, M.; Cao, X.; Yuan, Y.; Sun, L.; Xiang, B. Analyses on Climate Suitability of Capillary Heat Exchange System Metro Running Tunnel. *Acta Energiae Solaris Sin.* **2021**, *42*, 53–60. [CrossRef]
28. Vasilyev, G.P.; Peskov, N.V.; Lysak, T.M. Heat balance model for long-term prediction of the average temperature in a subway tunnel and surrounding soil. *Int. J. Therm. Sci.* **2022**, *172*, 107344. [CrossRef]
29. Hu, Z.; Geng, S.; Huang, Y.; Ge, F.; Wang, Y. Heat storage characteristics and application analysis of heat source tower in soil thermal balance of ground source heat pump. *Energ. Build.* **2021**, *235*, 110752. [CrossRef]

30. Liu, W.; Liang, S.; Shi, C. Risk modelling and simulation of thermal safety in underground railway tunnel surrounding. *Accid. Anal. Prev.* **2022**, *168*, 106620. [CrossRef] [PubMed]

31. Liu, W.; Zhou, Y.; Liang, S.; Liu, X.; Qin, Y. Analysis on heat storage in tunnel surrounding rock of subway under effects of periodic ground temperature-airflow temperature. *J. China Saf. Sci.* **2021**, *31*, 62–68. [CrossRef]

32. Wang, L.; Wang, W. Annual Dynamical Simulation of Temperature Field in Rock Surrounding Subway Tunnel. *Urban. Mass. Transit.* **2014**, *17*, 15–19. [CrossRef]

33. Liu, Y. Research on the heat sink of subway tunnel-heat sink effects caused by the periodic change of the ambient temperature. *J. Railw. Eng. Soc.* **2018**, *35*, 92–96. [CrossRef]

34. Du, Y.; Yang, X.; Yan, C. Numerical analysis of tunnel temperature field in seasonal frozen regions. *J. Glaciol. Geocryol.* **2017**, *39*, 366–374.

35. Rotta Loria, A. The thermal energy storage potential of underground tunnels used as heat exchangers. *Renew. Energ.* **2021**, *176*, 214–227. [CrossRef]

36. Wang, L.; Zuo, H.; Kong, M.; Ma, C.; Mao, Z.; Zeng, X.; Yin, L.; Cheng, J. Study on the evolution characteristics of temperature and heat storage of the soil surrounding the tunnel with years. *Energ. Build.* **2022**, *257*, 111804. [CrossRef]

37. Song, H.; Chen, Q. Dimensionless analysis of soil temperature field of shallow subway tunnel. *Energ. Build.* **2022**, *259*, 111900. [CrossRef]

38. Fu, Y.; Hu, J.; Wu, Y. Finite element study on temperature field of subway connection aisle construction via artificial ground freezing method. *Cold Reg. Sci. Technol.* **2021**, *189*, 103327. [CrossRef]

39. Peng, B.; Wu, X.; Zheng, Y. Analysis and Research on Influencing Factors of Thermal Environment in Metro Running Tunnel. *Build. Energ. Environ.* **2010**, *29*, 14–17. [CrossRef]

40. Hu, Z.; Li, X.; Zhao, X.; Xiao, L.; Wu, W. Numerical analysis of factors affecting the range of heat transfer in earth surrounding three subways. *J. China Univ. Min. Technol.* **2008**, *18*, 67–71. [CrossRef]

41. Wang, L.; Zhang, Y.; Du, Z.; Zhang, Y.; Gao, R.; Zheng, Y.; Song, J. Simulation study on the influence factors of thermal characteristics of surrounding rocks in subway tunnels. *Int. J. Refrig.* **2019**, *40*, 135–143. [CrossRef]

42. Qin, Y.; Jia, J.; Liu, W.; Yang, X. Four finite volume schemes for heat transfer problems. *J. Liaoning Technol. Univ. Nat. Sci.* **2013**, *32*, 763–767.

43. Qin, Y.; Meng, J.; Jia, J.; Yang, X.; Liu, W. Unsteady heat transfer problems with finite volume method. *J. Liaoning Technol. Univ. Nat. Sci.* **2013**, *32*, 577–581.

44. Zhang, X.; Ren, Z.; Mei, F. *Heat Transfer Theory*; China Construction Industry Press: Beijing, China, 2007; pp. 19–24.

45. Wang, H.; Wu, H.; Ding, Y.; Feng, J.; Wang, S. Feasibility and optimization of aerogel glazing system for building energy efficiency in different climates. *Int. J. Low-Carbon. Tec.* **2015**, *10*, 412–419. [CrossRef]

46. Ministry of Construction of the People's Republic of China. *Code for Design of Metro (GB 50157-2003)*; China Architecture and Building Press: Beijing, China, 2003.

47. Yang, Y.; Liu, F.; Xing, L.; Wang, H. Correlations and Variations between the initial average shallow ground temperature and the annual average ambient temperature. *J. Hebei Univ. Technol.* **2022**, *51*, 72–77. [CrossRef]

48. Wu, H.; Zhu, D.; Sun, J. Numerical simulation of the heat transfer in an earth-air heat exchange system. *J. South China Univ. Technol. Nat. Sci. Ed.* **2004**, *32*, 24–27. [CrossRef]

49. Qin, Y.; Wang, H.; Guo, K.; Xue, P.; Wang, J.; Wu, J. Simulation of finite volume method and experimental analysis for temperature field of roadway surrounding rock. *J. China Coal Soc.* **2017**, *42*, 3166–3175. [CrossRef]

50. Han, G.; Guo, Z. The speed at which heat is transferred (the movement of heat). In Proceedings of the 2006 Heat and Mass Transfer Conference of Chinese Society of Engineering Thermophysics, Chongqing, China, 19–22 October 2006.

51. Qin, Y.; Song, H.; Wu, J.; Bai, Y.; Dong, Z.; Ye, F. Analysis of surrounding rock heat dissipation for trapezoid roadway by finite volume method. *J. Liaoning Technol. Univ. Nat. Sci.* **2015**, *34*, 898–904.